

Magnetism, optical, and thermoelectric response of $CdFe_2O_4$ by using DFT scheme

Q Mahmood, M Yaseen, K C Bhamu, Asif Mahmood, Y Javed, Shahid M Ramay
Citation: Chin. Phys. B . 2018, 27(3): 037103. **doi:** 10.1088/1674-1056/27/3/037103

Journal homepage: http://cpb.iphy.ac.cn; http://iopscience.iop.org/cpb

What follows is a list of articles you may be interested in

Structural, electronic, and mechanical properties of cubic TiO_2: A first-principles study

Debashish Dash, Chandan K Pandey, Saurabh Chaudhury, Susanta K Tripathy
Chin. Phys. B . 2018, 27(1): 017102. **doi:** 10.1088/1674-1056/27/1/017102

Tuning electronic properties of the S_2/graphene heterojunction by strains from density functional theory

Jun-Hui Lei(雷军辉), Xiu-Fen Wang(王秀峰), Jian-Guo Lin(林建国)
Chin. Phys. B . 2017, 26(12): 127101. **doi:** 10.1088/1674-1056/26/12/127101

Strain engineering of electronic and magnetic properties of Ga_2S_2 nanoribbons

Bao-Ji Wang(王宝基), Xiao-Hua Li(李晓华), Li-Wei Zhang(张利伟), Guo-Dong Wang(王国东), San-Huang Ke(柯三黄)
Chin. Phys. B . 2017, 26(5): 057102. **doi:** 10.1088/1674-1056/26/5/057102

New ternary superconducting compound $LaRu_2As_2$: Physical properties from density functional theory calculations

M A Hadi, M S Ali, S H Naqib, A K M A Islam
Chin. Phys. B . 2017, 26(3): 037103. **doi:** 10.1088/1674-1056/26/3/037103

Stability, electronic structures, and mechanical properties of Fe-Mn-Al system from first-principles calculations

Ya-Hui Liu(刘亚会), Xiao-Yu Chong(种晓宇), Ye-Hua Jiang(蒋业华), Jing Feng(冯晶)
Chin. Phys. B . 2017, 26(3): 037102. **doi:** 10.1088/1674-1056/26/3/037102

Magnetism, optical, and thermoelectric response of $CdFe_2O_4$ by using DFT scheme

Q Mahmood[1], M Yaseen[2,†], K C Bhamu[3], Asif Mahmood[4], Y Javed[2], and Shahid M Ramay[5]

[1] *Materials Growth and Simulation Laboratory, Department of Physics, University of the Punjab, Lahore* 54000, *Pakistan*
[2] *Department of Physics, University of Agriculture, Faisalabad* 38040, *Pakistan*
[3] *Department of Physics, Goa University, Goa* 403206, *India*
[4] *Chemical Engineering Department, College of Engineering, King Saud University, Riyadh, Saudi Arabia*
[5] *Physics and Astronomy Department, College of Science, King Saud University, Riyadh, Saudi Arabia*

(Received 24 October 2017; revised manuscript received 30 November 2017; published online 13 February 2018)

Comparative analysis of electronic, magnetic, optical, and thermoelectric properties of $CdFe_2O_4$, calculated by employing PBEsol + mBJ has been done. The PBEsol reveals metallic nature, while TB-mBJ illustrates ferromagnetic semiconducting behavior. The reasons behind the origin of ferromagnetism are explored by observing the exchange, crystal field, and John–Teller energies. The optical nature is investigated by analyzing dielectric constants, refraction, absorption coefficient, reflectivity, and optical conductivity. Finally, thermoelectric properties are elaborated by describing the electrical and thermal conductivities, Seebeck coefficient, and power factor. The strong absorption for the visible energy and high power factor suggest $CdFe_2O_4$ as the potential candidate for renewable energy applications.

Keywords: frustrated magnetism, density functional theory, John–Teller distortion, Hund's rule

PACS: 71.15.Mb **DOI:** 10.1088/1674-1056/27/3/037103

1. Introduction

The spinel oxides have attracted immense attention of the scientific community, during the past few decades, for their diverse material properties that are suitable for wide range of technological device applications.[1] Among various spinel oxides, $CdFe_2O_4$ is considered important due to its normal spinel structure that is composed of Cd^{+2} and Fe^{+3} ions located at the tetrahedral and octahedral sites, respectively.[2] The trivalent iron ions form pyrochlore lattice, due to considerable magnetic frustration arising from these antiferromagnetically interacting magnetic ions.[3] The experimental lattice constant of $CdFe_2O_4$ spinel oxide is 8.715 Å[4] with the cubic space group $Fd\bar{3}m$.

$CdFe_2O_4$ has been grown by using a variety of growth techniques for exploring versatile physical properties.[5–9] In a recent experimental report, $CdFe_2O_4$ nanoparticles grown by employing a chemical condensation technique revealed a band gap of 1.74 eV, and hysteresis loop was measured at ambient temperature, suggesting potential magnetic and optical device applications,[10] while $CdFe_2O_4$ nanoparticles previously prepared by microwave assisted technique had revealed antiferromagnetic nature.[11] Ferrimagnetic ordering in the nanostructured $CdFe_2O_4$ spinel with particle size 4–60 nm has been reported to arise due to spin-glass-like surface structure (having huge magnetic anisotropy) that was justified by formation of a mixed spinel exhibiting spin canting at A and B sites.[12] Random distribution of magnetic ions in sputtered thin film of $CdFe_2O_4$ spinel has been verified to arise due to annealing. It enhances magnetic properties because of spin-glass-like structure stabilization.[13]

As technologically interesting material properties can be elaborated by theoretical computations, density functional theory (DFT) investigation becomes more relevant as desired conditions can be imposed onto the materials to comprehensively investigate the resulting characteristics. To the best of our knowledge, the DFT studies on $CdFe_2O_4$ have been seldom reported. For example, Fe–Fe interactions up to the third neighbor, as investigated by using generalized gradient approximation (GGA) and GGA+U (U is on-site Coulomb interaction), have been reported to operate within the geometrically frustrated cadmium ferrites.[14] Interestingly, third-neighbor interactions were found similar to the first-neighbor interactions.[14] A comparison between Trans-Blaha-modified-Becke-Johnson (TB-mBJ) and GGA+U is applied to investigate optical and magnetic characteristics of $CdFe_2O_4$. Both methods generate the consistent material parameters with the experiments.[15] In addition, no report exists in the literature that covers the thermoelectric properties of $CdFe_2O_4$.

As there have not been thorough investigations on the physical properties of $CdFe_2O_4$, we compare PBEsol functional with TB-mBJ potential by using DFT. The electronic, magnetic, optical, and thermoelectric properties produced by applying PBEsol functional and then mBJ potential are elaborated to demonstrate striking device applications.

†Corresponding author. E-mail: myaseen_taha@yahoo.com

© 2018 Chinese Physical Society and IOP Publishing Ltd

2. Calculation method

In this article, we have used the relaxed structure of cubic spinel oxide $CdFe_2O_4$ for strain minimization, and then optimization is done by using FP-LAPW method implemented into Wien2K code.[16] The optimized structure is used for total energy convergence by applying PBEsol[17] functional, and further applying modified Becke and Johnson potential as suggested by Trans and Blaha (TB-mBJ).[18] The selection of PBEsol and TB-mBJ potential is due to the inefficiency of GGA and LDA method in computing the consistent parameters with the experiments.[19,20] The TB-mBJ has quality to improve the electronic structure and band gap that are resonate with the experiments. In TB-mBJ potential, deviations due to GGA and LDA functional are averaged to approach closely to the experimental values. The parameter c (self-consistently converged value) is employed according to

$$V_{x,\sigma}^{\mathrm{mBJ}}(r) = cV_{x,\sigma}^{\mathrm{BR}}(r) + (3c-2)\frac{1}{\pi}\frac{\sqrt{5}}{12}\frac{\sqrt{2t_\sigma(r)}}{\rho_\sigma(r)}, \tag{1}$$

where $\rho_\sigma(r)$, $V_{x,\sigma}^{\mathrm{BR}}(r)$, and $t_\sigma(r)$ show DOS, Becke–Roussel potential, and K. E, respectively. The c is given by

$$c = \alpha + \left(\beta\frac{1}{V_{\mathrm{cell}}}\int \mathrm{d}^3r\frac{|\nabla\rho(r)|}{\rho(r)}\right)^{1/2}. \tag{2}$$

Here, the free parameters are $\alpha = -0.012$ and $\beta = 1.023$ Bohr$^{1/2}$.[18] For computing the electronic properties, firstly PBEsol is applied, and then, modified Becke-Johnson (mBJ) potential is employed. The use of mBJ is justified for its repute in calculating band gap that agrees to the experiments.

For the self-consistent process, inside and outside the atomic cores, relativistic spherical harmonic type and semi-relativistic approaches are employed respectively. A basis set is employed for controlling the wave function, potential and charge density in the muffin-tin region. The product of muffin-tin sphere radius and the plane-wave cut off in the reciprocal lattice is $R_{\mathrm{MT}} \times k_{\max} = 8$. The values of Gaussian vector $G_{\max}$ and angular momentum vector $l_{\max}$ are 20 (Ry)$^{1/2}$ and 10 respectively. An optimum number of k-points is used for generating a k-mesh of the order 20×20×20. The iteration process results total energy convergence up to 10^{-2} mRy. The Boltzmann kinetic transport theory and rigid band approach, as used in BoltzTrap code,[21,22] are applied to elucidate the thermoelectric properties. Therefore, the conductivity that is based on transport coefficient can be written as

$$\sigma_{\alpha\beta}(\varepsilon) = \frac{1}{N}\sum_{i,k}\sigma_{\alpha\beta}(i,k)\frac{\delta(\varepsilon-\varepsilon_{i,k})}{\delta(\varepsilon)}, \tag{3}$$

$$\sigma_{\alpha\beta}(i,k) = e^2\tau_{i,k}\upsilon_\alpha(i,\boldsymbol{k})\upsilon_\beta(i,\boldsymbol{k}), \tag{4}$$

where N shows number of k-points and τ is the relaxation time. The transport coefficients like electrical conductivity and Seebeck coefficient can be calculated by integrating the transport distribution function

$$\sigma_{\alpha\beta}(\alpha,\mu) = \frac{1}{\Omega}\int\sigma_{\alpha\beta}(\varepsilon)\left[-\frac{\partial f_0(T,\varepsilon,\mu)}{\partial\varepsilon}\right]\mathrm{d}\varepsilon, \tag{5}$$

$$S_{\alpha\beta}(T,\mu) = \frac{1}{eT\Omega\sigma_{\alpha\beta}(T,\mu)} \times\int\sigma_{\alpha\beta}(\varepsilon)(\varepsilon-\mu)\left[-\frac{\partial f_0(T,\varepsilon,\mu)}{\partial\varepsilon}\right]\mathrm{d}\varepsilon. \tag{6}$$

Here α and β illustrate tensor vectors, e, μ, Ω, and f_0 show electron charge, carrier concentration, unit cell volume, and Fermi–Dirac distribution function, respectively. Hence, Seebeck depends upon the electronic structure, while electrical conductivity is sensitive to the relaxation time.

3. Results and discussion

The computations are performed to determine the electronic structures for describing the magnetism in terms of exchange mechanism and John Teller effect. Similarly, optical and various thermoelectric parameters are also computed to reveal energy-related device applications.

3.1. Electronic structure and John–Teller distortion

The relaxed $CdFe_2O_4$ structure has been optimized in ferromagnetic (FM) and antiferromagnetic (AFM) states, and stable FM state is confirmed due to more energy released in FM state than in AFM state. While calculating the AFM, the nearest neighbor layers are flipped in alternative layer to add the spin contribution. The calculated ground state energy in AFM state for all configurations is compared with FM state energy. Stability of FM state is further confirmed due to negative sign of computed enthalpy of formation, as listed in Table 1.

Table 1. Various parameters calculated for $CdFe_2O_4$ in the FM state by using PBEsol and PBEsol + mBJ potentials.

Properties	PBEsol	PBEsol + mBJ	Experimental/Others
a_o/Å	8.71	8.70	Exp. 8.715[a], Theo. 8.69[c]
ΔE/meV	3.4	–	
Hf/eV	–1.77	–	
$\varepsilon_1(0)$	6.64	3.52	
$n(0)$	2.57	1.87	
$R(0)$	0.1945	0.0929	
ΔE_g/eV	–	1.86	Exp. 1.76[b], Theo.1.80[d]
Δ_{JT}	1.49	0.64	
$\Delta_x(d)$	3.81	6.79	
$\Delta_x(pd)$	0.00	–0.600	
ΔE_C/eV	0.1476	–2.575	
ΔE_V/eV	0.6260	–0.706	
$N_o\alpha$	0.0367	–0.643	
$N_o\beta$	0.1565	-0.176	
M_{tot}/μ_B	18.00	19.99	Theo. 19.99[d]
M_{Cd}/μ_B	0.09	0.97	
M_O/μ_B	2.51	4.06	
M_{Fe}/μ_B	14.0	11.15	
M_{Int}/μ_B	3.89	2.32	

[a]Ref. [4], [b]Ref. [10], [c]Ref. [15], [d]Ref. [50].

Hence, compound $CdFe_2O_4$ keeps less energy as compared to the sum of the atomic state energies of Cd, Fe, and O. The ground state parameters like lattice constant, bulk modulus and its pressure derivative calculated through Morgan's equation of state are also listed in Table 1. The electronic structure of the studied compound which is revealed through PBEsol functional shows metallic behavior, while TB-mBJ improves the electronic structure and ferromagnetic semiconducting nature, as can be seen in Figs. 1 and 2, respectively. The spin polarization P is extracted by using $P = \frac{N\downarrow - N\uparrow}{N\downarrow + N\uparrow} \times 100$, where $N\uparrow$ and $N\downarrow$ show electron densities at E_F in respective spin orientations. The applications of TB-mBJ suggest that spin polarization reduces to zero (in computations with PBEsol that was nonzero due to metallic nature) because in both spin channels no state crosses E_F.[23–25]

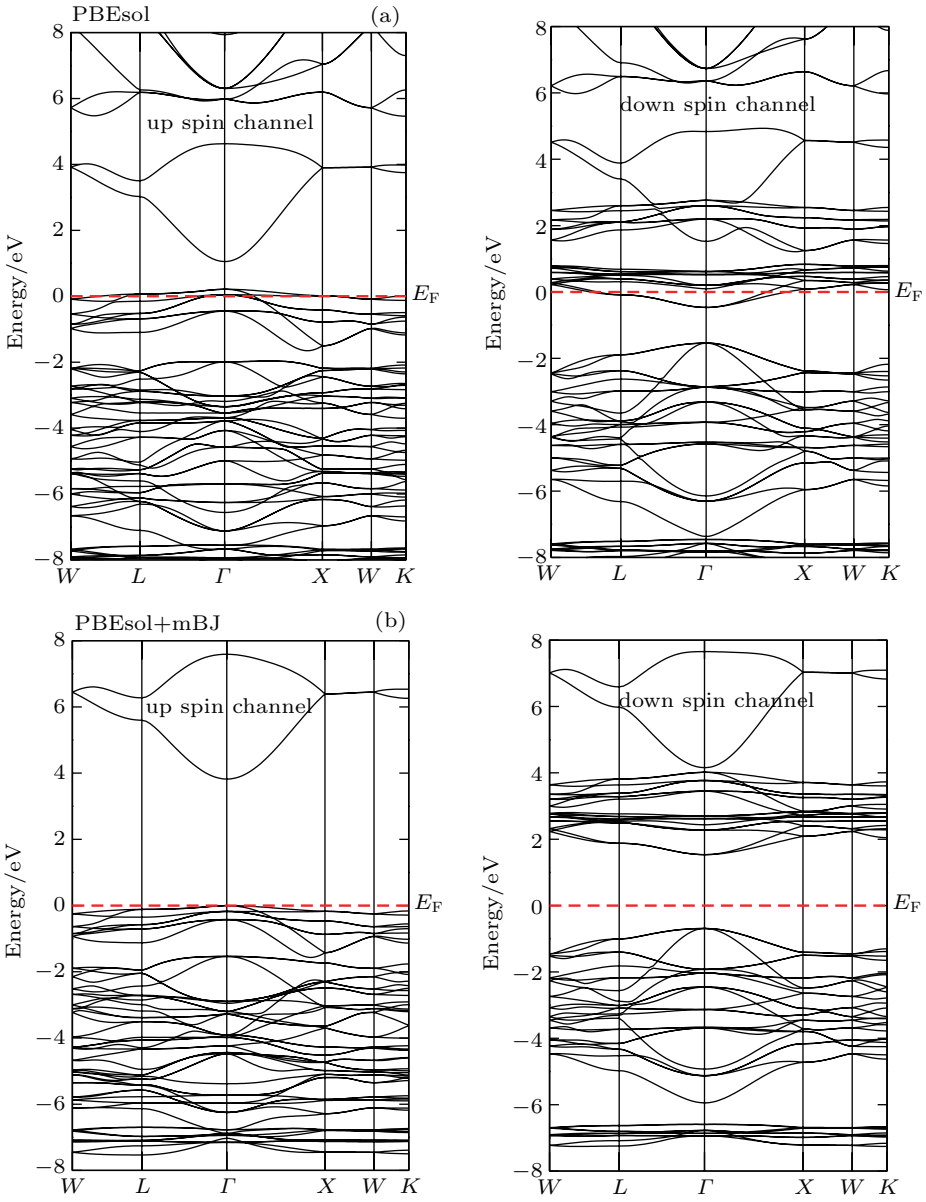


Fig. 1. (color online) Spin polarized band structures of $CdFe_2O_4$ computed by applying PBEsol and PBEsol + mBJ functional.

The band structures (BS) and density of states (DOS) computed by using TB-mBJ potential, as shown in Figs. 1(a), 1(b), 2(a), and 2(b), illustrate that $CdFe_2O_4$ is ferromagnetic semiconductor because both spin channels show direct band gap (E_g) at the Gamma point in the first Brillion zone and no state crosses E_F. The depletion of states and appearance of E_g around E_F in both spin channels are due to the exchange interactions. The presence of exchange interactions is evident because of unequal shift in energy in the spin polarized electronic structures, suggesting that the illustrated semiconducting behavior is also associated with a stable ferromagnetic state. On the other hand, computations performed through solely PBEsol show metallic response, for in both spin channels states cross E_F. the Fermi level moves, for spin up channel inside the valence band and for spin down channel inside the conduction band. Therefore, the holes for up spin

channel and electrons for down spin channel are available for conduction process. To reveal the origin of ferromagnetism in detail, total and partial density of states are presented in Figs. 2(a) and 2(b). When computations are done by using TB-mBJ potential, the Fe d-states hybridize with O p-states in the energy region from 2 eV to 4 eV in the conduction band for down spin channel, and −1 eV to −5 eV in the valence band for up spin channel, while this hybridization energy range is contracted when PBEsolis is used. Basically, exchange splitting of 3d-states of Fe appears, due to octahedral environment of oxygen (FeO_6) causing a net crystal field, as schematically shown in Fig. 3. The crystal field splits the 3d-states into doublet e_g ($d_{x^2-y^2}$) and d_{z^2} and triplet states t_{2g} (d_{xy}, d_{yz}, and d_{zx}), with increased and decreased energy respectively.[26–28] The degenerate orbitals can be suppressed through symmetry reductions, and this could be achieved by elongation or stretching bonds along z-axis, which are named as Z-out and Z-in distortions respectively. Therefore, orientation of the bonds and lowering symmetry make t_{2g} and e_g states strongly non-degenerate, thus distorting the octahedral symmetry into tetragonal one, as shown in Fig. 3. Because of that, d_{z^2}, d_{yz}, and d_{zx} orbitals are lowered in energy but $d_{x^2-y^2}$ and d_{xy} orbitals has raised energy. This effect elongates the bond along z-direction, which is the preferred direction, and usually occurs when degeneracy in the e_g level with orbitals d^4, d^7, d^8, etc. occurs. The Fe atom has seven valence electrons in the 3d-state, therefore, such elongations are preferred. To investigate the details of the (John Teller) JT distortions, the crystal field and JT energies are calculated by the relations; $(\Delta_{CF}^{\uparrow} = t_{2g}^{\uparrow} - e_g^{\uparrow})$ for up, $(\Delta_{CF}^{\downarrow} = t_{2g}^{\downarrow} - e_g^{\downarrow})$ for down spin channel, and $(\Delta_{JT} = \Delta_{CF}^{\uparrow} - \Delta_{CF}^{\downarrow})$ respectively. The values are presented in Table 1. Here $\Delta_{CF}^{\uparrow}$ and $\Delta_{CF}^{\downarrow}$ represent the crystal field energy for spin up and spin down channels. The direct exchange energy $(\Delta_{EX}(d) = \Delta_d^{\downarrow} - \Delta_d^{\uparrow}))$ and indirect exchange energy $(\Delta_{EX}(pd) = E_V^{\downarrow} - E_V^{\uparrow})$ due to Fe-3d spin orientations are also calculated and reported in Table 1. The comparison of crystal field and John–Teller energies with the exchange energies $((\Delta_{EX}(d) \geq \Delta_{CF} \geq \Delta_{JT})$ depicts strong role of exchange interactions.[29–33] The negative indirect exchange energy $\Delta_{EX}(pd)$ suggests that the dominant character of electronic spin is to form the more attractive spin down channel, as the reduced energy is more evident through the computations done by using PBEsol + mBJ potential. At the same time, computing indirect exchange energy through PBEsol potential gives out zero, which is due to the metallic nature. Similarly, using PBEsol + mBJ potential instead of PBEsol improves direct exchange energy and reduces John Teller energy. The magnetic moments of compound and individual atoms like Fe, Cd and O calculated by using PBEsol functional and TB-mBJ potential are listed in Table 1.

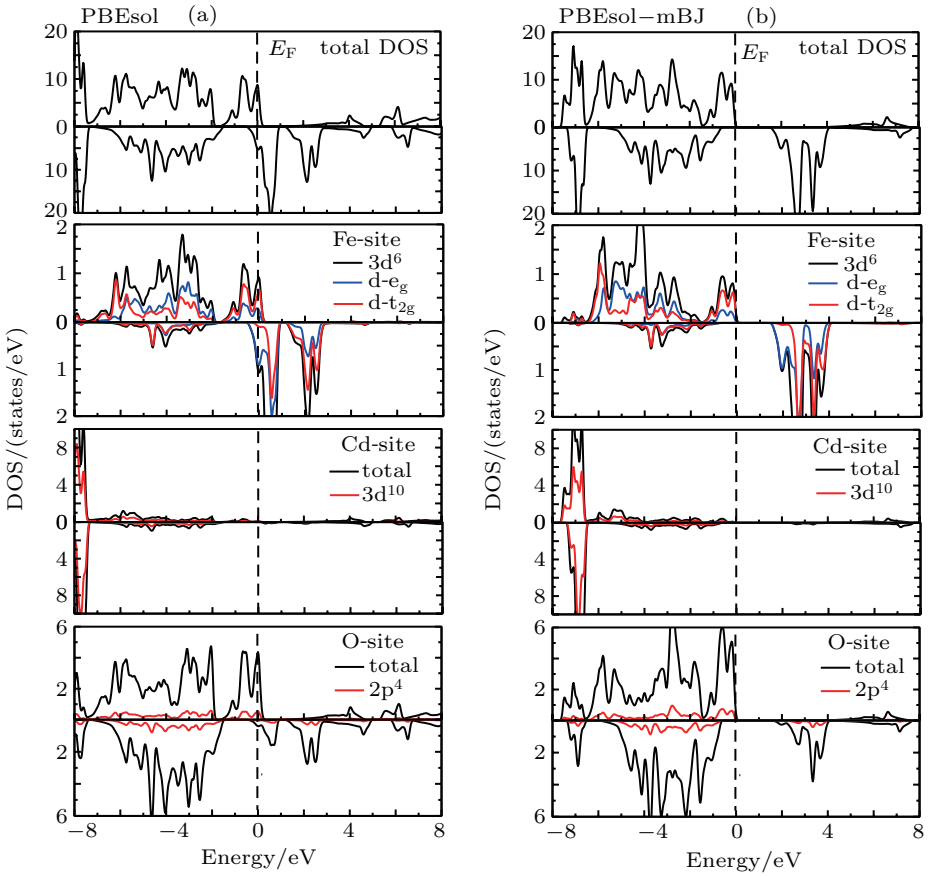


Fig. 2. (color online) (a), (b) Total (TDOS) and partial density of states (PDOS) determined for $CdFe_2O_4$ for both spin configuration by applying PBEsol and PBEsol + mBJ functional.

The magnetic moment with PBEsol functional is an integer while for TB-mBJ potential is a fractional, and that gives the evidence of convergence of metallic to semiconductor. The reduction of magnetic moment of Fe and its sharing to the nonmagnetic sites elucidate the strong hybridization between 3d-states of Fe and 2p-states of O. Computations through TB-mBJ illustrate that shifting of magnetic moment from magnetic to nonmagnetic site is stronger as compared to the computations through PBEsol functional. It suggests that in the studied compound, exchange mechanism is more favored in the ferromagnetic semiconducting than in the metallic compounds. The magnetic moments determined by the varying symmetries such as $Fd3m$, $P3m1$, and $Pnma$ are 19.99 μ_B, 199 μ_B and 40 μ_B, respectively. The computed magnetic moment for $P3m1$ phase is higher, but being the lowest for $Fd3m$ phase, while computed enthalpy of formations shows that $CdFe_2O_4$ has the highest stability in $Fd3m$ phase, and this is the reason we have preferred to study the cubic phase of $CdFe_2O_4$.[32,33]

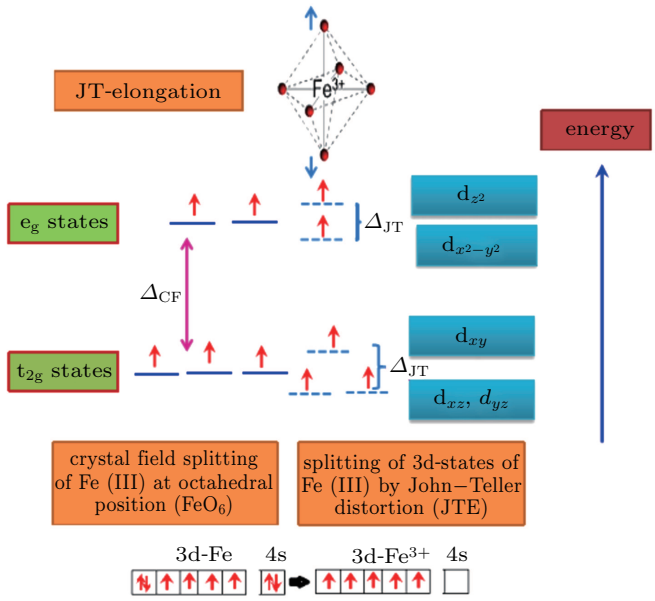


Fig. 3. (color online) The splitting of 3d-states of Fe (III) by John Teller distortion (JTE) at octahedral position in the spinel structure of $CdFe_2O_4$.

3.2. Optical behavior

The details of the electronic transitions, illustrating material interactions with the impinging radiations w.r.t. in various symmetry directions of the first Brillion zone are observed through inter-and intra-band transitions, which cause varying excitation and de-excitation rates. While, the inter-band transitions are sufficient for precisely revealing the optical behaviors, and can be expressed by complex dielectric constant $\varepsilon(\omega = \varepsilon_1(\omega) + i\varepsilon_2(\omega)$.[34–37] The real part, $\varepsilon_1(\omega)$, shows dispersion, while imaginary part, $\varepsilon_2(\omega)$, indicates light absorption, and both are related through Kramer–Kronig relation.[38] Both $\varepsilon_1(\omega)$ and $\varepsilon_2(\omega)$ are of fundamental importance because of being used to compute many other optical parameters.[36,37] We have applied PBEsol and PBEsol + mBJ potential to determine various optical parameters, within 0–10 eV, as illustrated in Figs. 4–5. The $\varepsilon_1(\omega)$ determined by PBEsol and PBEsol + mBJ are plotted in Fig. 4. It is evident that $\varepsilon_1(\omega)$ computed by using PBEsol potential reaches maximum at 1.76 eV. After attaining minimum at 3.18 eV, it again becomes maximum at 4.06 eV. The large intensity peaks depict sharply altering polarization to exhibit plasmonic excitations, of which appearance is due to the metallic nature. In contrast, using PBEsol + mBJ potential shows linearly enhancing $\varepsilon_1(\omega)$ up to 3.7 eV, and if it is above this energy, it decreases to the minimum without any considerable features. This is caused by the semiconducting characters. Hence, mBJ potential improves the band gap, as already shown in Fig. 1. From 5.8 eV to 8.2 eV, $\varepsilon_1(\omega)$, when using PBEsol potential to compute, it becomes negative, revealing reflective nature to the incoming radiations. While PBEsol + mBJ potential does not expose this fact. Interestingly, static dielectric constant $\varepsilon_1(0)$ and E_g (computed by using PBEsol and PBEsol + mBJ potentials) have been found to satisfy Penn's relation $\varepsilon_1(0) \approx 1 + (h\omega_p/E_g)^2$,[39] as shown in Table 1.

The $\varepsilon_2(\omega)$, showing absorptive nature for the incoming radiations, exhibits a threshold energy for the absorption, which are 1.43 eV and 2.36 eV, after calculating with PBEsol and PBEsol + mBJ respectively. The metallic response due to PBEsol potential shows sharp peaks in $\varepsilon_2(\omega)$, induced by different resonance frequencies. This is evident in the computed band structure having states crossing E_F in both spin channels (see Fig. 1). Owing to the semiconducting character as elucidated through PBEsol + mBJ potential, both channels ignore the presence of free carries, due to which, $\varepsilon_2(\omega)$ uniformly improves with energy and shows maximum absorption at 4.7 eV, and then also uniformly deceases to minimum, as shown in Fig. 4(b).

The refractive index $n(\omega)$ and extinction coefficient $k(\omega)$, as plotted in Figs. 4(c) and 4(d), show a nature similar to that determined for $\varepsilon_1(\omega)$ and $\varepsilon_2(\omega)$. These parameters are related according to the relations $n^2 - k^2 = \varepsilon_1(\omega)$ and $2nk = \varepsilon_2(\omega)$.[40] The refractive index $n(\omega)$ shows transparency while extinction coefficient $k(\omega)$ describes light attenuating capability of a material. The zero frequency limits for $\varepsilon_1(\omega)$ and $n(\omega)$, illustrated as and $n(0)$ respectively, satisfying the relation . The values of and $n(0)$ are higher for PBEsol potential than PBEsol + mBJ potential because the later potential improves the band, making the material more suitable to the optoelectronic applications.

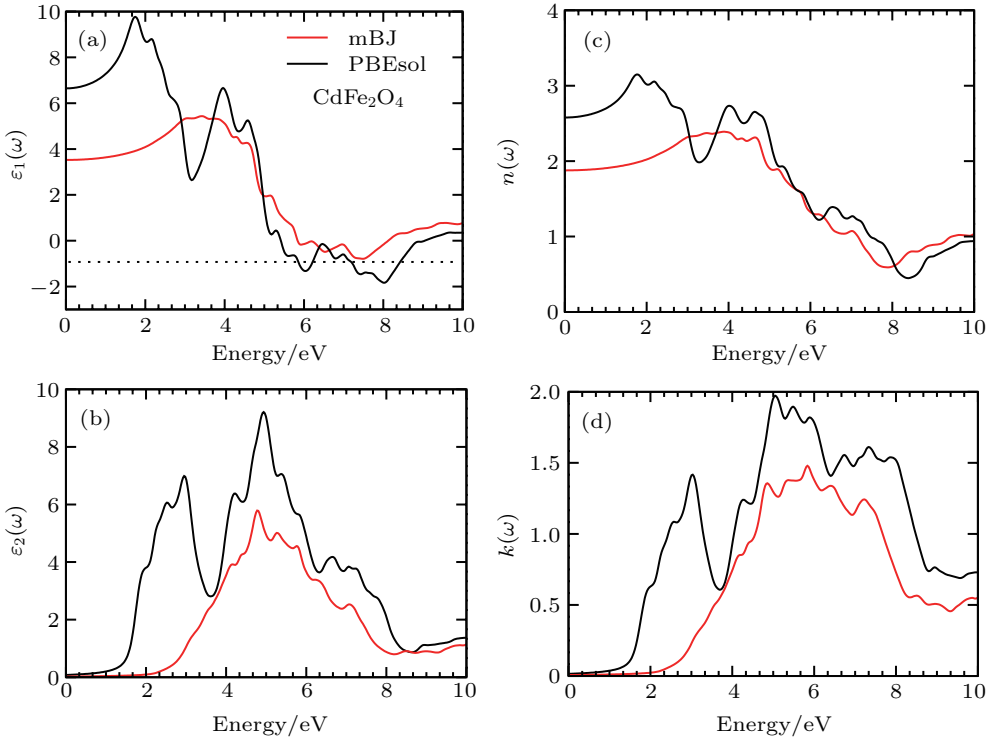


Fig. 4. (color online) (a) Real $\varepsilon_1(\omega)$ and (b) imaginary $\varepsilon_2(\omega)$ dielectric constants, (c) refractive index $n(\omega)$ and extinction co-efficient $k(\omega)$ calculated for $CdFe_2O_4$ in FM phase by employing PBEsol and PBEsol + mBJ functional.

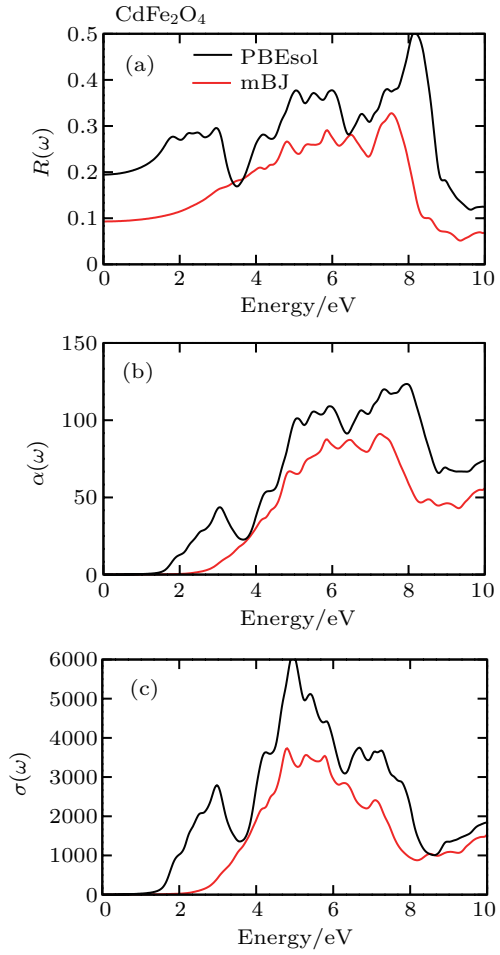


Fig. 5. (color online) (a) Reflectivity, (b) absorption coefficient, and (c) optical conductivity calculated for $CdFe_2O_4$ in FM phase by employing PBEsol and PBEsol + mBJ functional.

To probe surface quality, light reflected by the material surface is observed by computing reflectivity $R(\omega)$ using PBEsol and PBEsol + mBJ potentials, as presented Fig. 5. There are large variations in the $R(\omega)$ determined by using PBEsol, as compared to that determined by using PBEsol + mBJ potentials, and it is again due to electronic structure difference that varies the carrier distribution. The $R(0)$ determined through PBEsol + mBJ potential (0.0929) is much smaller than extracted through PBEsol potential (0.195), suggesting optoelectronic applications. Similarly, absorption coefficient $\alpha(\omega)$ showing light absorption, as depicted in Fig. 5(b), exhibits critical values of 1.43 eV and 2.36 eV after applying PBEsol and PBEsol + mBJ potential, respectively. It agrees well to the $\varepsilon_2(\omega)$, $k(\omega)$, and E_g values (extracted from the band structures, E_g is taken from the difference of valence band maxima and conduction minima, although the available carries for PBEsol make the studied compound metallic like system), showing the precision of the results. Moreover, according to the relation, $\alpha(\omega) = 4\pi k(\omega)/\lambda$, photons having shorter wavelength ($E_g = hc/\lambda$) than a critical value are more susceptible to absorption, suggesting the significant role of PBEsol + mBJ potential in elucidating those critical values for suggested attractive optical applications.[41]

The optical conductivity, $\sigma(\omega)$, showing optically activated free charge carriers, is computed by using both potentials, as expressed in Fig. 5(c). A part of impinging photons energy equal to E_g is consumed by the material, while remaining energy ($hf > E_g$) is responsible in generating free carriers (electrons and holes) to induce a forward current. As being ex-

pected, $\sigma(\omega)$ computed by using PBEsol potential illustrates more carriers for conduction than that computed by employing PBEsol + mBJ potential (because it showed semiconducting nature). Hence, the use of mBJ potential improves the band statures to enhance the feasibility of optical applications.

3.3. Thermoelectric properties

The imbalanced demand and supply chain of energy has stimulated researchers to search for the materials exhibiting high waste heat for useful energy conversion efficiencies. Such thermoelectric materials are gauged in terms of high electrical conductivity (σ/τ) and low thermal conductivity (κ/τ), to enhance the power factor $(\mathrm{PF} = \sigma S^2/\kappa)$ and the figure of merit or the thermal efficiency $(\mathrm{ZT} = \sigma S^2 T/k)$, where S is Seebeck coefficient and τ is relaxation time.[42–46] Mostly, in semiconductors, σ and S exhibit opposite trend. The thermoelectric nature of $CdFe_2O_4$ is investigated by computing σ, S, electronic part of the thermal conductivity κ_e and PF, within 200–800 K, and are plotted in Figs. 6(a)–6(d). The semi-classical theory based on BoltzTraP code[47] is used for these computations. As shown in Fig. 6(a), electrical conductivity linearly increases from 0.52×10^{18} $(\Omega{\cdot}\mathrm{m}{\cdot}\mathrm{s})^{-1}$ to 5.0×10^{18} $(\Omega{\cdot}\mathrm{m}{\cdot}\mathrm{s})^{-1}$ by increasing temperature from 200 to 800 K respectively. This could be justified by the fact that increasing temperature enhances thermal energy of the electrons to freely form a high conducting state.

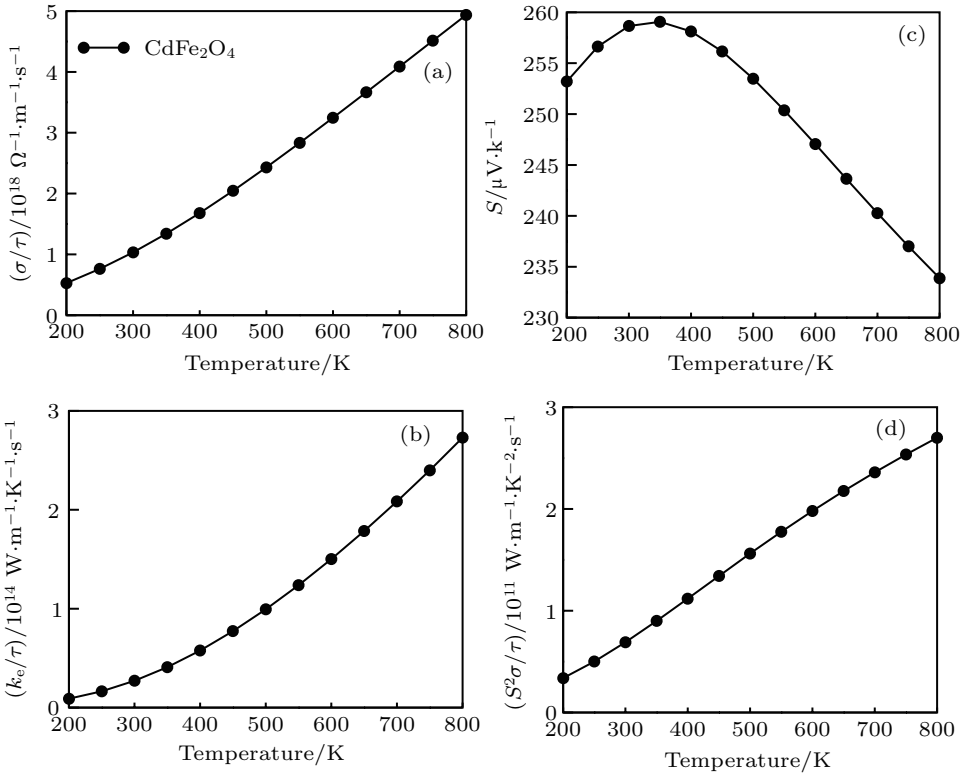


Fig. 6. (a) Electrical conductivity, (b) Seebeck coefficient, (c) thermal conductivity, and (d) power factor extracted for $CdFe_2O_4$ by applying BoltzTraP code.

As total thermal conductivity (κ/τ) arises due to both electrons and phonons, the Fourier law, written as $q = -\kappa \mathrm{d}T/\mathrm{d}x$ (q and $\mathrm{d}T/\mathrm{d}x$ illustrate heat flow per unit time and the temperature gradient), can describe the thermal conductivity.[48] The electronic thermal conductivity also linearly improves from 0.1×10^{14} (W/m·K·s) to 2.8×10^{14} (W/m·K·s) by increasing temperature from 200 K to 800 K (see Fig. 6(b).

It is important to notice a potential difference (ΔV) due to temperature gradients (ΔV), because the ratio of ΔV and ΔT expresses the Seebeck coefficient (S) that is useful in deciding the efficiency of a thermocouple. The S computed for $CdFe_2O_4$ is plotted in Fig. 6(c). It is evident in Fig. 6(c), that S initially increases with temperature and reaches 259 μV/K at 350 K. Above that, it decreases linearly and becomes 235 μV/K at 800 K. The decaying Seebeck coefficient may be due to the negative coefficient of temperature in typical semiconductors. Power factor (PF), which is related to the product of σ and square of S, is very useful to reveal thermoelectric application, and is also computed and presented in Fig. 6(d). As can be observed in Fig. 6(d), PF linearly increases from 0.3×10^{11} W/m·K^2·S to 2.8×10^{11} W/m·K^2·s with rising temperature from 200 K to 800 K. Therefore, linearly increasing PF having very high magnitude suggests the potential in $CdFe_2O_4$ for commercial thermoelectric applications.[49]

4. Conclusions

The density functional theory based on Wien2K code is applied for describing the electronic, magnetic and optical behaviors of $CdFe_2O_4$ by applying PBEsol and PBEsol + mBJ potentials. Thermoelectric properties computed by BoltzTrap code are also presented. Following important conclusions are drawn.

(i) The comparison of ground state energies in FM and AFM states confirms stable FM state, which is further verified by the negative enthalpy of formation.

(ii) The electronic behaviors illustrate metallic and semiconducting nature, according to the computations done by using PBEsol and PBEsol + mBJ potential, respectively.

(iii) The computed exchange energies are found higher than crystal field and John–Teller distortions evidence stable FM state. Similarly, negative *pd*-exchange energy shows strong hybridization elucidating the dominant role of the carrier spin.

(iv) The use of mBJ potential reveals that band gap operates in the visible energy revealing $CdFe_2O_4$ as s suitable candidate for optoelectronic industry.

(v) The computed PF exhibits very large values suggesting $CdFe_2O_4$ to be suitable for various applications, such as thermoelectric generators and refrigerators.

Acknowledgement

The authors acknowledge Prof. K R Priolkar, Goa University and C-DAC, Pune for providing research and computing facilities. They would like to extend sincere appreciations to the Deanship of Scientific Research at King Saud University for the research group project (Grant No. RGP-311). K C Bhamu wishes to acknowledge UGC for financial support (Dr. D. S. Kothari Postdoctoral Fellowship, Grant No. PH/13–14/0113). M Yaseen is thankful to Higher Education Commission (HEC), Pakistan for financial support (Grant No. 6410/Punjab/NRPU/R&D/HEC/2016).

References

[1] Valenzuela R 2012 *Physics Research International* 2012 591839
[2] Arean C O, Diaz E G, Gonzalez J M R, Garcia M A 1988 *J. Solid. Stat. Chem.* **77** 275
[3] Yafet Y and Kittel C 1952 *Phys. Rev. B* **87** 290
[4] Kamazawa K, Park S, Lee S H, Sato T J and Tsunoda Y 2004 *Phys. Rev. B* **70** 024418
[5] Nayak P K 2008 *Mater. Chem. Phys.* **112** 24
[6] Yokoyama M, Ohta E and Satoo T 1998 *J. Magn. Magn. Mater.* **183** 173
[7] Mahmoud M H, Abdallas A M, Hamdeh H H, Hikal W M, Taher S M and Ho J C 2003 *J. Magn. Magn. Mater.* **263** 269
[8] Lou X, Liu S, Shi D and Chu W 2007 *Mater. Chem. Phys.* **105** 67
[9] Miao F, Deng Z, Lv X, Gu G, Wan S, Fang X, Zhang Q and Yin S 2010 *Solid State Commun.* **150** 2036
[10] Sagadevan S, Pal K, Chowdhury Z Z and Hoque M E 2017 *Mater. Res. Express* **4** 075025
[11] Vasanthi V, Shanmugavani A, Sanjeeviraja C and Selvan R K 2012 *J. Magn. Magn.Mater.* **324** 2100
[12] Chinnasamy C N, Narayanasamy A, Ponpandian N, Joseyphus R J, Chattopadhyay K, Shinoda K, Jeyadevan B, Tohji K, Nakatsuka K and Greneche J M 2001 *J. Appl. Phys.* **90**
[13] Akamatsu H, Zong Y, Fujiki Y, Kamiya K, Fujita K, Murai S and Tanaka K 2008 *IEEE Transaction. Magnetic.* **44** 2796
[14] Cheng C 2008 *Phys. Rev. B* **78** 132403
[15] Zaari H, El Hachimi A G, Benyoussef A and El Kenz A 2015 *J. Magn. Magn. Mater.* **393** 183
[16] Blaha P, Schwarz K, Madsen G K H, Kvasnicka D and Luitz J 2001 *WIEN2K, an augmented plane wave+local orbitals program for calculating crystal properties*, Karlheinz Schwarz, Techn. Universitat, Vienna, Austria
[17] Blaha P, Schwarz K, Sorantin P and Trickey S K 1990 *Comput. Phys. Commun.* **59** 339
[18] Tran F and Blaha P 2009 *Phys. Rev. Lett.* **102** 226401
[19] van de Walle A and Ceder G 1999 *Phys. Rev. B* **59** 14992
[20] Perdew J P, Chevary J A, Vosko S H, Jackson K A, Pederson M R, Singh D J and Fiolhais C 1992 *Phys. Rev. B* **46** 6671
[21] Scheidemantel T J, Ambrosch-Draxl C, Thonhauser T, Badding J V and Sofo J O 2003 *Phys. Rev. B* **68** 125210
[22] Hosseini S M 2008 *Phys. Stat. Sol.* **245** 2800
[23] Zhang J, Li X and Yang J 2015 *J. Mater. Chem. C* **3** 2563
[24] Wen C and Yan S 2010 *J. Appl. Phys.* **107** 043913
[25] Saini H S, Singh M, Reshak A H and Kashyap M K 2013 *J. Magn. Magn. Mater.* **331** 1
[26] Walsh A, Wai S H, Yan Y, Al-Jassim M M and Turner J A 2007 *Phys. Rev. B* **76** 165119
[27] Varignon J, Bristowe N C and Ghosez P *Sci. Rep.* **5** 15364
[28] Jeng H T, Lin S H and Hsue C S 2006 *Phys. Rev. Lett.* **97** 067002
[29] Choi H C, Shim J H and Min B I 2006 *Phys. Rev. B* **74** 172103
[30] Kumar A, Fennie C J and Rabe K M 2012 *Phys. Rev. B* **86** 184429
[31] Kant C, Deisenhofer J, Tsurkan V and Loidl A 2010 *J. Phys: Conf. Seri.* **200** 032032
[32] Ramay S M, Hassan M, Mahmood Q and Mahmood A 2017 *Current Appl. Phys.* **17** 1038
[33] Mahmood Q, Hassan M, Ahmed S H A, Bhamu K C, Mahmood A and Ramay S M J *Matt. Chem. Phys. Solid*
[34] Khan M A, Kashyap A, Solanki A K, Nautiyal T and Auluck S 1993 *Phys. Rev. B* **48** 16974
[35] Fox M 2001 *Optical Properties of Solids*, Oxford University Press ISBN: 9780199573370
[36] Mahmood Q, Hassan M and Noor N A 2016 *J. Phys.: Condens. Matter* **28** 506001
[37] Mahmood Q and Hassan M 2017 *J. Alloy. Compond.* **704** 659
[38] Marius G 2010 Kramers-Kronig Relations (The Physics of Semiconductors) (Berlin Heidelberg: Springer) p. 775
[39] Penn D 1962 *Phys. Rev. B* **128** 2093
[40] Mahmood Q, Alay-e-Abbas S M, Hassan M and Noor N A 2016 *J. Alloy. Compond.* **688** 899
[41] Peng C and Gao L 2008 *J. Am. Ceram. Soc.* **91** 2388
[42] Biswas K, He J, Blum I D, Wu C I, Hogan T P, Seidman D N, Dravid V P and Kanatzidis M G 2012 *Nature* **489** 414
[43] Goldsmid H J and Douglas R W 1954 *Br. J. Appl. Phys.* **5** 386
[44] Tritt T M 2011 *Rev. Mater. Res.* **41** 433
[45] Ruleovaa P, Drasar C, Lostak P, Li C P, Ballikaya S and Uher C 2010 *Mater. Chem. Phys.* **119** 2991
[46] Qu X, Wang W, Liu W, Yang Z, Duan X and Jia D 2011 *Mater. Chem. Phys.* **129** 331
[47] Madsen G K H, Schwarz K and Singh D J 2006 *Comput. Phys. Commun.* **175** 67
[48] Liu C and Morelli D T 2011 *J. Elect. Mat.* **40** 678
[49] Ramachandran T, Rajeevan N E and Pradyumnan P P 2013 *Mater. Sci. Appl.* **4** 816
[50] Saal J E, Kirklin S, Aykol M, Meredig B and Wolverton C 2013 *Materials Design and Discovery with High-throughput Density Functional Theory: the Open Quantum Materials Database* (oqmd), JOM 65 (11), pp. 1501–1509